

# Higher-Order Meta Distribution Analysis of Wireless Systems with Application to the Reliability of UWB THz Networks

Mehdi Monemi, *Member, IEEE*, Mehdi Rasti, *Senior Member, IEEE*, S. Ali Mousavi, *Fellow, IEEE*, Matti Latva-aho, *Fellow, IEEE*, Martin Haenggi, *Fellow, IEEE*

**Abstract**—Communication reliability, as defined by 3GPP, refers to the probability of providing a desired quality of service (QoS). This metric is typically quantified for wireless networks by averaging the QoS success indicator over spatial and temporal random variables. Recently, the meta distribution (MD) has emerged as a two-level performance analysis tool for wireless networks, offering a detailed examination of the outer level (i.e., system-level) reliability assessment versus the inner level (i.e., link-level) reliability thresholds. Most existing studies focus on first-order spatiotemporal MD reliability analyses, and the benefits of leveraging MD reliability for applications beyond this structure remain unexplored, a gap addressed in this paper. We present wireless application examples that can benefit the higher-order MD reliability analysis. Specifically, we provide the analysis and numerical results for a second-order spatial-spectral-temporal MD reliability of ultra-wideband THz communication. The results demonstrate the value of the hierarchical representation of MD reliability across three domains and the impact of the inner-layer target reliability on the overall MD reliability measure.

**Index Terms**—Meta distribution, reliability, wireless networks, THz wideband communication.

## I. INTRODUCTION

Traditional reliability analyses of wireless networks often rely on calculating the success probability across all random variables involved in the performance measure using techniques such as stochastic geometry. This can be mathematically formulated as  $\mathbb{P}_{\mathcal{X}}(Q > q)$  where  $Q$  is the quality-of-service (QoS) function,  $q$  is the desired threshold value, and  $\mathcal{X}$  is the collection of all random elements of the system. This approach, while straightforward, is limited in its ability to capture the intricate dependencies and uncertainties inherent in complex wireless environments. By considering the calculation of success probabilities in a hierarchical scheme, the meta distribution (MD) provides insights into the variability and uncertainty associated with the network performance [1], [2]. Splitting the collection of random elements into ordered classes of  $\mathcal{X}_0$  and  $\mathcal{X}_1$ , the (first-order) MD reliability calculates

the overall reliability measure as  $\mathbb{P}_{\mathcal{X}_1}(\mathbb{P}_{\mathcal{X}_0}(Q > q | \mathcal{X}_1) > p_1)$  where  $p_1$  is a given target reliability value. The inner and outer probabilities can be interpreted as link-level and system-level reliability measures in wireless networks [3]. This provides information about the distribution of the conditional success probability of the typical link which is an important parameter to be evaluated for mobile network operators (MNOs) [4]. Therefore, the MD reliability allows for a more comprehensive understanding of how inner-layer reliability measures contribute to the overall network performance. MD-based analyses have been leveraged for wireless networks in many of the existing works. In the context of performance evaluation and reliability analysis, several works have investigated the characterization and calculation of signal-to-interference (SIR) or signal-to-interference-plus-noise (SINR) meta distribution. The MD of SIR for Poisson network models was initially introduced and evaluated in [5]. Subsequent research extended the results to various device-to-device (D2D) and cellular networks [6]–[8]. In addition to SIR, several studies have investigated the MD of SINR and rate for Poisson network models. For example, in [9], the MD of the secrecy rate of a single node in the presence of randomly located eavesdroppers was investigated. In [10] the MD of the downlink rate of the typical UAV under base station (BS) cooperation in a cellular-connected UAV network was studied using a standard beta distribution approximation. The authors of [11] have investigated the rate MD in ultra-reliable low-latency communication (URLLC) D2D networks considering the errors due to the misalignment of radiated beams. In [12], the energy and rate MD have been leveraged to quantify a performance metric termed *wirelessly powered spatial transmission efficiency* for D2D networks. By formally characterizing the link and spatial reliability concepts and utilizing MD reliability analysis, the authors of [13] have derived closed-form formulations for bandwidth requirements needed for guaranteeing target values of link and spatial reliability in URLLC networks.

The study of MD is not limited to SIR, SINR, and rate in Poisson network models. Given the difficulty in analyzing non-Poisson network models, especially MD distributions, the authors of [4] proposed a simplified scheme called ASAPPP (“Approximate SIR Analysis Based on the Poisson Point Process”) to approximate the SIR MD for non-Poisson networks. Considering a clustering strategy for wireless devices around the access points (APs), the authors of [14] derived expressions for the MD of wireless energy transfer and wireless

Mehdi Monemi, Mehdi Rasti, and Matti Latva-Aho are with the Centre for Wireless Communications (CWC), University of Oulu, Oulu, Finland (emails: mehdi.monemi@oulu.fi, mehdi.rasti@oulu.fi, and matti.latva-aho@oulu.fi).

S. Ali Mousavi is with the Department of Electrical Engineering, Shiraz university of Technology, Shiraz, Iran (e-mail: al.mousavi@sutech.ac.ir).

Martin Haenggi is with the Department of Electrical Engineering, University of Notre Dame, Notre Dame, IN 46556 USA (e-mail: mhaenggi@nd.edu).

This work is supported by Business Finland via the 6GBridge - Local 6G project (grant number 8002/31/2022) and by 6G Flagship (Grant Number 369116) funded by the Research Council of Finland

information transfer to investigate the average proportion of the wireless devices in one cluster that achieves successful performance while satisfying the reliability constraint.

To the best of our knowledge, all existing related works in the literature investigating the MDs in wireless networks have focused on *first-order* spatiotemporal MD analysis, considering the random *spatial* distribution of the wireless nodes and the *temporal* characteristics of the per-link small-scale fading channels. In this work, characterize and analyze higher-order MD reliabilities and provide application examples wherein the first-order or second-order MD reliability extends beyond traditional spatiotemporal domains. The main contributions of this work are listed as follows:

- We formally express the zeroth-order (non-MD) and first-order MD reliability representation and provide examples of wireless applications where MD reliability characterization extends beyond the conventional spatiotemporal domain that has been widely explored and discussed in the literature.
- Building on the strengths of first-order MD analyses of the reliability, we present the higher-order MD reliability representation wherein the random variables are partitioned into multiple ordered classes and the reliability analysis is conducted hierarchically across several domains. Wireless application examples are presented that leverage higher-order MD analyses to conduct a multi-level study of the system's reliability.
- We study the second-order *temporal-spectral-spatial* MD reliability in wideband frequency-hopping spread spectrum (FHSS) THz networks. Our approach incorporates the statistics of small-scale fading channels, the spectral characteristics of FHSS carriers, and the spatial distribution of wireless nodes into a unified MD reliability framework. This is the first application of a higher-order MD analysis. It gives important understanding about the interplay between target threshold values on the MD reliability and provides insight into balancing spectrum allocation to achieve optimal spatial MD reliability while meeting temporal and spectral reliability targets.

The remainder of the paper is structured as follows. Section II investigates the conventional (non-MD) and first-order MD reliability analysis and provides examples in wireless applications where first-order spatiotemporal and non-spatiotemporal MD reliability analysis can be leveraged. Section III extends the MD reliability characterization for higher-order MDs and provides a related application example. Section IV investigates the analysis of the second-order temporal-spectral-spatial MD reliability for ultra-wideband THz networks. Finally, the paper is concluded in Section V.

## II. NON-MD AND FIRST-ORDER MD-BASED RELIABILITY ANALYSIS

In this section, we study the conventional non-MD reliability as well as first-order MD reliability in wireless networks. We provide 3 spatiotemporal examples (Examples 1-3 shown in Fig. 1), which will be extended in the next section for beyond first-order spatiotemporal MD reliability applications (Examples 4-6 shown in Fig. 1).

### A. Conventional (non-MD) Reliability

The communication reliability, as defined by 3GPP [15], refers to the success probability of delivering  $l$  bits with a time delay lower than a user-plane deadline threshold  $t_{\text{th}}$ . Although primarily introduced for low-latency services (such as URLLC), it applies to different network services including URLLC, enhanced mobile broadband (eMBB), and massive machine-type communication (mMTC). This definition can further be generalized as follows to encompass a broader range of applications:

*Definition 1:* The reliability measure  $R$  is the probability that the QoS measure function  $Q$  be higher than a minimum required threshold  $q$ , i.e.,

$$R(q) = \mathbb{P}_{\mathcal{X}}(Q > q), \quad (1)$$

where  $\mathcal{X}$  is the collection of random elements including *temporal* random variables (e.g., small-scale fading), *spatial* random variables (if any, such as the stochastic point process corresponding to the positions of users/BSSs), or any additional random variables across different dimensions. The QoS function  $Q$  may be formulated in various forms depending on the service type and system model.

*Example 1: Conventional stochastic geometry based reliability analysis for URLLC services:* Consider a downlink communication scenario where a set of users and BSs are randomly scattered in the network region according to a stationary Poisson point process (PPP). Each user is provided with URLLC service through the nearest BS with packets of  $l$  bits at time duration  $t_l$  obtained from the Shannon-Hartley capacity. We have  $t_l(\text{SINR}(\mathcal{H}, \Phi)) = l/(W \log(1 + \text{SINR}(\mathcal{H}, \Phi)))$ , where  $\mathcal{H}$  and  $\Phi$  are the random variables corresponding to small-scale fading channels and the point process relating to the users'/BSs' locations respectively, and  $W$  is the bandwidth. The reliability is obtained as  $R = \mathbb{P}(1/t_l(\text{SINR}(\mathcal{H}, \Phi)) > 1/t_{\text{th}})$ . For the simple case of orthogonal frequency carriers where the interference is negligible relative to noise through coordinating the frequency resources in nearby cells, and considering that all links follow same channel fading statistics, the function  $\text{SINR}(\mathcal{H}, \Phi)$  can be replaced by the simpler signal-to-noise-ratio (SNR) function  $\text{SNR}(\mathcal{H}, \mathcal{R})$  where  $\mathcal{H}$  is the scalar small-scale fading of the typical link and  $\mathcal{R}$  is the length of the typical link. Considering the independence of the spatial and temporal distributions, the reliability is then obtained as  $\iint_{(h,r) \in \mathcal{S}} f_{\mathcal{H}}(h) f_{\mathcal{R}}(r) dh dr$ , where  $f_{\mathcal{H}}(h)$  is the probability density function (pdf) of the fading channel for each of the users,  $f_{\mathcal{R}}(r) = 2\pi\lambda r e^{-\lambda\pi r^2}$  is the pdf of the distance  $\mathcal{R}$ ,  $\lambda$  is the intensity of the PPP, and finally  $\mathcal{S}$  is the region of interest characterized as  $\mathcal{S} = \{(h, r) \in \mathbb{R}_+^2 \mid t_l(\text{SNR}(h, r)) \leq t_{\text{th}}\}$ . Here, the SNR function can be modeled as  $\text{SNR}(h, r) = \frac{P_{\text{T}} G_{\text{T}} G_{\text{R}} c^2}{(4\pi f)^2} \times \frac{hr^{-\alpha}}{N_0 W}$ , where  $c$  is the speed of light,  $f$  is the frequency,  $\alpha$  is the path loss exponent,  $W$  is the bandwidth,  $N_0$  is the spectral density of the noise,  $P_{\text{T}}$  is the transmit power, and  $G_{\text{T}}$  and  $G_{\text{R}}$  are the transmit and receive antenna gains, respectively.

### B. First-Order Spatiotemporal MD Reliability

To provide a hierarchical reliability analysis, the first-order MD reliability is defined as follows:

*Definition 2:* Assume that the collection of random variables  $\mathcal{X}$  is partitioned into the ordered classes  $\mathcal{X}_0$  and  $\mathcal{X}_1$ . Given the two parameters  $q$  and  $p_1 \in [0, 1]$ , the (first-order) MD reliability measure is defined as<sup>1</sup>

$$R^{\text{MD}}(p_1; q) = \mathbb{P}_{\mathcal{X}_1}(\mathbb{P}_{\mathcal{X}_0}(Q > q \mid \mathcal{X}_1) > p_1), \quad (2)$$

where  $p_1$  is the first-level target reliability value.

From (2) it is seen that  $R^{\text{MD}}(p_1; q)$  measures the probability of achieving the desired QoS conditioned on  $\mathcal{X}_1$  be higher than a threshold value  $p_1$ . For now, consider that  $\mathcal{X}_1$  and  $\mathcal{X}_2$  correspond to temporal and spatial random variables, respectively. Assuming  $\mathcal{X}_2$  to be an ergodic process, the MD reliability  $R^{\text{MD}}(p_1; q)$  captures the overall *spatial reliability* over the service region by guaranteeing the *link reliability* threshold of  $p_1$  over all realizations of spatial variables (e.g., locations of the users or BSs). The following example introduces a foundational system model that serves as the basis for reliability analysis conducted in many studies investigating the reliability of wireless communications following the meta distribution approach.

*Example 2: First-order MD Reliability for URLLC services [13]:* Consider the URLLC network service expressed in Example 1. Letting  $\mathcal{X}_0 = \mathcal{H}$  and  $\mathcal{X}_1 = \Phi$ , the MD reliability  $R^{\text{MD}}(p_1; q)$  results in the spatial reliability over a point process by considering that the link-level success probability of  $p_1$  is satisfied over all realizations of the corresponding point process.

The study of MD reliability in the spatiotemporal domains is not limited to delay-tolerant (e.g., URLLC) and rate-tolerant (e.g., eMBB) services, as exemplified in the following.

*Example 3: First-order MD reliability for the harvested energy analysis [12]:* Consider a collection of D2D devices scattered in the network with a spatial distribution described by some point process. The QoS function can be considered as the amount of harvested energy during each time slot, denoted by  $\mathcal{E}$ , which can be formulated as a function of fading channels  $\mathcal{H}$  and users' positions corresponding to  $\Phi$  [12]. The energy harvesting MD reliability  $R^{\text{MD}}$  is obtained as the meta distribution of the harvested energy  $\mathcal{E}(\mathbf{h}, \phi)$  guaranteeing the link energy success probability higher than the threshold  $p_1$  conditioned on spatial positions of users and RF transmitters which follows a spatiotemporal MD analysis similar to Example 2.

### C. First-Order Non-Spatiotemporal MD Reliability

As previously mentioned, similar to Example 2, the majority of existing studies in the field formulate and scrutinize the first-order MD reliability, taking into account that the inner and outer layers correspond to the time and space domains, respectively. However, in practical scenarios, a multitude of system models and problem formulations exist where MD reliability can be utilized in a different domain configuration. The subsequent example presents such a case.

*Example 4: End-to-end link reliability leveraging the MD of radio-link and Fronthaul/Backhaul Connections:* Consider a

<sup>1</sup>. While the subscripts of  $\mathbb{P}$  in (2) are technically redundant, we retain them for enhanced clarity. This holds for the subscript of  $\mathbb{P}$  in (1) as well.

Non-MD reliability	First-order MD reliability		Section II
Example 1	Example 2,3	Example 4	
$\mathcal{X} = \{\mathcal{H}, \Phi\}$ Spatiotemporal	$\mathcal{X}_0 = \mathcal{H}$ Temporal $\mathcal{X}_1 = \Phi$ Spatial	$\mathcal{X}_0 = \mathcal{H}$ Temporal $\mathcal{X}_1 = \mathcal{T}$ Temporal	
Second-order MD reliability			Sections III, IV
Example 5	Case study		
$\mathcal{X}_0 = \mathcal{H}$ Temporal $\mathcal{X}_1 = \mathcal{V}$ Spatiotemporal $\mathcal{X}_2 = \Phi$ Spatial	$\mathcal{X}_0 = \mathcal{H}$ Temporal $\mathcal{X}_1 = \mathcal{F}$ Spectral $\mathcal{X}_2 = \Phi$ Spatial		

Fig. 1: Example scenarios presented in this work for the non-MD, first-order MD, and second-order MD reliability analyses.

URLLC network service wherein an end-to-end connection is set between a fixed user and the associated access point. The end-to-end delay can be modeled as  $t = t_l(\text{SINR}(\mathcal{H}, \Phi_0)) + \mathcal{T}$ , where  $t_l$  is the radio link delay corresponding to the transmission of the packet of  $l$  bits from the user to the access point (e.g., gNodeB),  $\Phi_0$  is the set of locations of the network nodes, which are assumed to be fixed, and  $\mathcal{H}$  denotes the small-scale fading channel of the links, and  $\mathcal{T}$  is the additional delay due to queuing, routing, processing, etc. in the fronthaul/backhaul of the network, relating to the connection from the access point to the final destination (e.g., user plane function (UPF)). By considering the radio link reliability of  $p_1$ , and assuming a statistical model for  $\mathcal{T}$ , the overall MD reliability is calculated according to (2) where  $\mathcal{X} = \{\mathcal{H}, \mathcal{T}\}$ , in which  $\mathcal{H} \equiv \mathcal{X}_0$  and  $\mathcal{T} \equiv \mathcal{X}_1$ . For the case of orthogonal multiple access where no interference is imposed from other links, similar to Example 1, the function  $\text{SINR}(\mathcal{H}, \Phi_0)$  reduces to  $\text{SNR}(\mathcal{H}; R_0)$  where  $\mathcal{H} \in \mathcal{H}$  is the scalar small-scale fading of the intended communication link, and  $R_0$  is the distance of the link which is assumed to be a fixed here. Given  $t_{\text{th}}$  and  $p_1$ , the MD reliability can be obtained as

$$\begin{aligned} R^{\text{MD}} &= \mathbb{P}_{\mathcal{T}}(\mathbb{P}_{\mathcal{H}}(t < t_{\text{th}} \mid \mathcal{T}) > p_1) \\ &= \mathbb{P}_{\mathcal{T}}(\mathbb{P}_{\mathcal{H}}(t_l(\text{SNR}(\mathcal{H}; R_0)) + \mathcal{T} < t_{\text{th}} \mid \mathcal{T}) > p_1) \\ &= \bar{F}_{\bar{F}_{\mathcal{H}}(\text{SNR}^{-1}(t_l^{-1}(t_{\text{th}} - \mathcal{T}); R_0) | \mathcal{T})}(p_1), \end{aligned} \quad (3)$$

where  $\text{SNR}^{-1}(\gamma; R_0) = \{h \mid \text{SNR}(h; R_0) = \gamma\}$  and  $\bar{F}_X$  denotes the complementary cumulative distribution function (ccdf) of  $X$ . Note that the small-scale fading random variable  $\mathcal{H}$  and the random delay process  $\mathcal{T}$  corresponding to the fronthaul/backhaul transmission are both temporal random variables. Note that  $\mathcal{H}$  and  $\mathcal{T}$  can be considered uncorrelated in most practical scenarios.

### III. BEYOND FIRST-ORDER MD RELIABILITY ANALYSES

Most studies in the literature use a first-order MD reliability framework with spatiotemporal decomposition as exemplified in Examples 2 and 3. However, the MD's applicability in wireless network reliability extends beyond this. Building on the strengths of first-order MD analyses of the reliability over space and time domains, we extend this to a broader, higher-order MD reliability analysis over various domains.

This allows for a more nuanced understanding of reliability across different dimensions. For instance, higher-order MD analyses can capture complex interactions between factors like signal strength variations, delay jitter, fading, frequency statistics, and packet loss variations. By analyzing these dependencies in a hierarchical structure, we can gain valuable insights into resource allocation strategies and improve network performance prediction, leading to more robust and reliable wireless networks, in the sense that the impact of a change in the reliability measure at each dimension can be accurately monitored and explored in the overall reliability of the system.

Formally, higher-order MDs are defined as follows:

*Definition 3:* Let  $Q$  be a function of random elements  $\mathcal{X}$ , which are partitioned into the ordered classes  $\mathcal{X}_0, \dots, \mathcal{X}_n$ . Let the random variables  $P_1, \dots, P_n$  iteratively be

$$\begin{aligned} P_1 &\triangleq \mathbb{P}_{\mathcal{X}_0}(Q > q) = \mathbb{P}(Q > q \mid (\mathcal{X}_1, \mathcal{X}_2, \dots, \mathcal{X}_n)) \\ P_2 &\triangleq \mathbb{P}_{\mathcal{X}_1}(P_1 > p_1) = \mathbb{P}(P_1 > p_1 \mid (\mathcal{X}_2, \mathcal{X}_3, \dots, \mathcal{X}_n)) \\ &\vdots \\ P_n &\triangleq \mathbb{P}_{\mathcal{X}_{n-1}}(P_{n-1} > p_{n-1}) = \mathbb{P}(P_{n-1} > p_{n-1}). \end{aligned} \quad (4)$$

The  $k$ -th order MD is defined as

$$R_{[k]}(\mathbf{p}_k, q) \triangleq \mathbb{P}(P_k > p_k), \quad k \in [n], \quad (5)$$

where  $\mathbf{p}_k \triangleq (p_1, \dots, p_k) \in [0, 1]^k$ . Besides, we call  $R_{[n]}(\mathbf{p}_n, q)$  (equivalently denoted by  $R^{\text{MD}}(\mathbf{p}_n, q)$ ) the ( $n$ -th order) MD reliability measure, which can be expressed compactly as

$$\begin{aligned} R^{\text{MD}}(\mathbf{p}_n, q) &\triangleq \mathbb{P}(P_n > p_n) = \\ P_{\mathcal{X}_n} &(P_{\mathcal{X}_{n-1}}(\dots(P_{\mathcal{X}_1}(Q > q) > p_1) > \dots > p_{n-1}) > p_n). \end{aligned} \quad (6)$$

*Remark 1:* The  $k$ -th order MD for  $k < n$  is effectively only based on a partition of size  $k + 1$  since  $\mathcal{X}_k, \dots, \mathcal{X}_n$  are lumped together and expected over in the last step of calculating  $\mathbb{P}(P_k > p_k)$ . Hence the partition is  $\mathcal{X}_0, \dots, \mathcal{X}_{k-1}, \mathcal{X}_k^n$ , where  $\mathcal{X}_k^n = (\mathcal{X}_k, \dots, \mathcal{X}_n)$ .

*Remark 2:* Since  $\mathbb{E}(P_k) = \mathbb{P}(P_{k-1} > p_{k-1})$  the MDs are related as

$$R_{[k-1]}(\mathbf{p}_{k-1}, q) = \int_0^1 R_{[k]}(\mathbf{p}_k, q) dp_k. \quad (7)$$

*Remark 3:* Note that removing the outermost layer of  $R_{[n]}$  in (6) which results in  $P_{\mathcal{X}_{n-1}}(\dots(P_{\mathcal{X}_1}(Q > q) > p_1) > \dots > p_{n-1})$  does not yield the  $(n - 1)$ -th order MD since it is a function of  $\mathcal{X}_n$ .

*Remark 4:* A compact form of higher-order MD representation was introduced in [2]. However, that definition does not establish a relationship between the MDs of different order. In this paper, we have extended that representation in the context of MD reliability and presented a hierarchical form of MDs in (4) and (5), where MDs are iteratively related according to (7). This approach enhances the understanding of how the MD at each domain influences MDs in other domains and provides an easier way to tract corresponding mathematical calculations for obtaining the overall MD reliability, as evidenced in Appendix I.

TABLE I: Parameters used for Numerical Results

Parameter	Description	Value
$(\underline{f}^{(2)}, \bar{f})$	Frequency range in Scenario 1	(340, 375) GHz
$(\underline{f}^{(1)}, \bar{f})$	Frequency range in Scenario 2	(325, 375) GHz
$\lambda$	Intensity of the PPP	$1.5 \times 10^{-3} \frac{1}{\text{m}^2}$
$(G_T, G_R)$	Transmit and receive antenna gains	(25, 25) dB
$W$	Bandwidth	1 GHz
$l$	No. of bits to be received in time $t_{\text{th}}$	1000
$t_{\text{th}}$	User-plane deadline threshold	10 $\mu\text{s}$
$K$	Rician shape factor	2
$P_T$	Transmit power	0.1 W
$k(f)$	Molecular absorption coefficient	See Fig. 1 in [9]

Next we give two examples wherein a second-order MD reliability analysis can be beneficial.

*Example 5: Application of MD to assess mobility-aware system reliability:* Mobility can significantly impact system reliability by introducing challenges like Doppler shifts and handoff delays. In practice, different users might have different velocities at different snapshots of time and spatial realizations of the point process, and thus the mobility can be modeled as a spatiotemporal random variable whose distribution may be uniform or Gaussian [16]. Consider a network scenario similar to Example 1, where we model the velocity of users as random variables denoted by  $\mathcal{V}$ . The QoS function can be expressed as  $Q(\mathcal{V}, \mathcal{H}, \Phi) = \delta(\mathcal{V})/t_l(\text{SINR}(\mathcal{H}, \Phi))$ , where  $\delta(\mathcal{V}) \leq 1$  captures the capacity reduction due to mobility-related issues, such as Doppler spread and the reduction of the channel coherence time. With the  $Q$  function and the information about the models and corresponding parameters of the random variables, the MD reliability is obtained using (6). Here, as shown in Fig. 1, we have  $\mathcal{X}_0 \equiv \mathcal{H}$ ,  $\mathcal{X}_1 \equiv \mathcal{V}$ , and  $\mathcal{X}_2 \equiv \Phi$ , where the corresponding random variables are represented in temporal, spatiotemporal and spatial domains, respectively.

#### IV. APPLICATION OF SPATIAL-SPECTRAL-TEMPORAL MD RELIABILITY FOR THz COMMUNICATION

In this section, we analyze the second-order MD reliability for ultra-wideband THz communication. The statistics of the carrier frequency might influence the overall reliability measure of a communication link. Incorporating the spectral domain in the reliability analysis is more significant when dealing with ultra-wideband (UWB) communications. For example, consider a UWB communication through frequency hopping spread spectrum (FHSS) where carriers assigned to users may vary over time according to a pseudorandom policy, spanning the entire available spectrum. This provides benefits such as security and robustness making the communication more resilient against interference and jamming. While the impact of frequency might be negligible in the reliability measure in applications requiring a low amount of spectrum, this is not the case for UWB applications.

Consider an FHSS UWB network of randomly located nodes communicating in THz band where each user is assigned a carrier frequency, selected deterministically from a pseudorandom sequence generated for that user. While the sequence generation process is deterministic, the resulting frequency

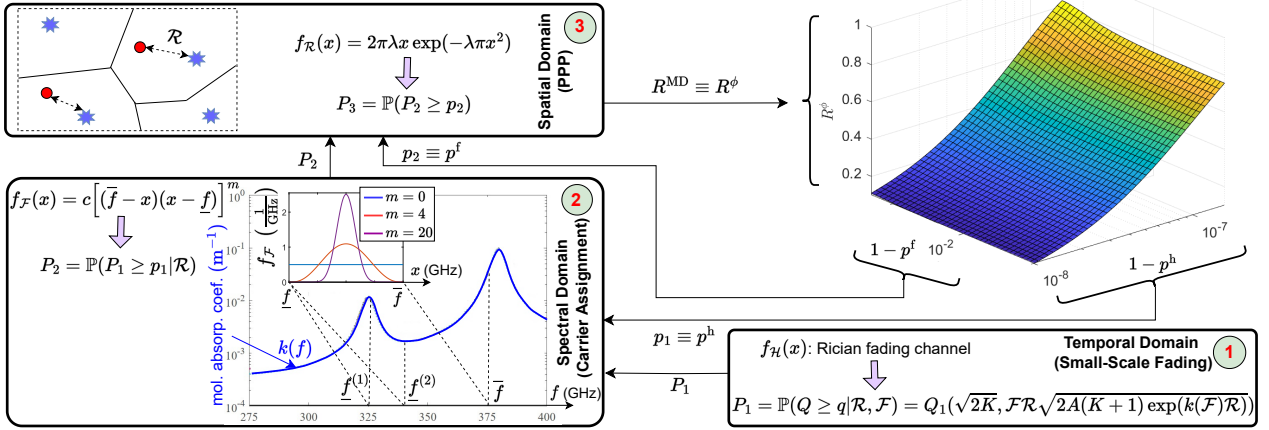


Fig. 2: The 3-level calculation and illustration of the MD reliability  $R^\phi$  versus  $p^f$  and  $p^h$

hopping pattern appears stochastic to an external observer, where the corresponding pdf is determined by the carrier assignment algorithm. Here the statistics of the varying carrier frequency can highly affect the reliability. This is because, the large-scale path loss is a function of the frequency, especially at THz bands where the molecular absorption is a frequency-dependent factor that highly affects the signal attenuation. Following Example 1, considering that co-channel interference is negligible and all links follow same channel fading statistics, we can express the MD reliability according to (6), where  $Q = 1/t_l(\text{SNR}(\mathcal{H}, \mathcal{F}, \mathcal{R}))$ , in which the ordered collections of random variable are  $\mathcal{X}_0 \equiv \mathcal{H}$ ,  $\mathcal{X}_1 \equiv \mathcal{F}$  and  $\mathcal{X}_2 \equiv \mathcal{R}$ . These are scalars corresponding to the small-scale fading, carrier frequency, and the distance between some user in the network and its nearest BS. For each user, the carrier frequency is a pseudorandom variable selected according to some pdf determined by the carrier assignment algorithm. Similar to Example 1 and considering the line-of-sight (LoS) THz channel model [17] as well as the simple case of orthogonal carrier allocation, we can formulate the user-plane latency  $t_l$  corresponding to  $l$  data bits at frequency  $f$  as

$$t_l = \frac{l}{W \log \left( 1 + \frac{P_{\text{Tx}} G_{\text{T}} G_{\text{R}} c^2}{(4\pi f)^2} \times \frac{hr^{-2} e^{-k(f)r}}{N_0 W} \right)}, \quad (8)$$

where  $r$  is the distance,  $k(f)$  is the molecular absorption coefficient at frequency  $f$ , and  $h$  is the the small-scale fading coefficient. We aim to calculate the MD reliability of delivering  $l$  bits with a time delay lower than a user-plane deadline threshold  $t_{\text{th}}$ , given the target temporal reliability  $p_1 \equiv p^h$  and target spectral reliability  $p_2 \equiv p^f$ .

We consider a THz network wherein BSs are scattered according to PPP with density  $\lambda$ , and each user is assigned to the nearest BS. Accordingly, the pdf of the distance is  $f_{\mathcal{R}}(r) = 2\pi\lambda r \exp(-\lambda\pi r^2)$ . We have adopted the molecular absorption coefficient according to Fig. 1 in [17] for the frequency range from  $\underline{f} = 275$  GHz to  $\bar{f} = 325$  GHz, where the corresponding coefficient  $k(f)$  is depicted in Fig. 2. We assume that each user is assigned a carrier frequency at each time step where the carrier is selected according to some pdf  $f_{\mathcal{F}}$  supported on  $[\underline{f}, \bar{f}]$ . The pseudorandom carrier assignment

is commonly considered to have uniform distribution  $U(\underline{f}, \bar{f})$  to allow effective spreading of the signal across the available bandwidth. To investigate the impact of frequency domain pseudorandom carrier assignment in the overall MD reliability measure, we adopt the more general model

$$f_{\mathcal{F}}(x) = c \left[ (\bar{f} - x)(x - \underline{f}) \right]^m, \quad (9)$$

where  $m$  is the shape factor and  $c = (\bar{f} - \underline{f})^{-1-2m} / \beta(1 + m, 1 + m)$  in which  $\beta$  is the beta function. As seen in Fig. 2, adjusting the shape factor  $m$  results in different pdf models. For  $m = 0$ , it is the uniform distribution, and as  $m \rightarrow \infty$ , it approaches the Dirac delta function at  $(\underline{f} + \bar{f})/2$ .

Finally in the temporal domain, noting that THz communication is mostly achieved in LoS for short regions, a Rician fading channel model with pdf  $f_{\mathcal{H}}$  having shape factor  $K$  is assumed. For the sake of simplicity, we are not including a blockage model for communication between the BS and user, as considered in some works in the literature [18], [19]. As depicted in Fig. 2 and considering (4), the MD reliability calculations can be achieved in three steps. In the first step, we formulate the temporal reliability as  $P_1 = \mathbb{P}(Q > q | \mathcal{R}, \mathcal{F})$ . Considering the Rician fading channel model and the representation of  $t_l$  for THz channels expressed in (8), after some mathematical manipulations (see Appendix I-A1),  $P_1$  can be obtained as

$$P_1 = Q_1(\sqrt{2K}, \mathcal{F}\mathcal{R}\sqrt{2c_1(K+1)\exp(k(\mathcal{F})\mathcal{R})}), \quad (10)$$

where  $c_1 = \frac{N_0 W (4\pi)^2}{P_{\text{Tx}} G_{\text{T}} G_{\text{R}} c^2} (2^{\frac{l}{W t_{\text{th}}}} - 1)$  and  $Q_1$  is the first-order Marcum Q-function. In the second step, given  $P_1$  and the target temporal-domain reliability  $p_1 \equiv p^h$ , and considering the adopted models for molecular absorption coefficient  $k(f)$  as well as the pdf for carrier assignment  $f_{\mathcal{F}}$ , we can formulate  $P_2 = \mathbb{P}(P_1 > p^h | \mathcal{R})$ . Finally, considering the pdf of  $f_{\mathcal{R}}$  obtained from PPP where  $\mathcal{R}$  is the distance between the user and the nearest BS, in the third step we can obtain  $R^{\text{MD}} \equiv R^\phi$  corresponding to a target spectral reliability  $p_2 \equiv p^f$  by solving  $P_3 = \mathbb{P}(P_2 > p^f)$ . The 3D MD reliability diagram for  $R^\phi$  versus  $p^h$  and  $p^f$  is depicted in Fig. 2. 2D representations of the MD reliability versus  $p^h$ ,  $p^f$ , and bandwidth (BW) are also presented in Figs. 3, 4, and 5, respectively. The parameter

values used for the numerical results are listed in Table I. We have considered two scenarios. In Scenario 1, corresponding to Figs. 3 and 4, we explore the MD reliability analysis for a fixed bandwidth of  $BW = \bar{f} - f^{(2)}$  corresponding to a *monotonically increasing* part of  $k(f)$  in the frequency range  $(\underline{f}^{(2)}, \bar{f})$ . In Scenario 2, we investigate the MD reliability analysis for a variable frequency range of  $(\underline{f}^{(1)}, \underline{f}^{(1)} + BW)$ , where  $BW \in [0, \bar{f} - \underline{f}^{(1)}]$  lies within a more general *non-monotonic* part of  $k(f)$ . The corresponding values considered for  $\underline{f}^{(1)}$ ,  $\underline{f}^{(2)}$  and  $\bar{f}$  are shown in Fig. 2 and Table I. An analytical closed-form solution for Scenario 1 and a low-complexity numerical solution scheme for Scenario 2 has been presented in Appendix I-A and Appendix I-B respectively. Several points are observed from the numerical results:

- First, it is seen how the spatial MD reliability measure is a monotonically decreasing function of both temporal and spectral reliability measures. For example, it is observed in Fig. 3 that for  $m = 0$  and  $p^h = 1 - 7 \times 10^{-8}$ , increasing  $p^f$  from 0.9 to 0.99 decreases the spatial MD reliability  $R^\phi$  from 0.8 to 0.74. The monotonically decreasing property is justified by noting that guaranteeing higher reliability measures in the temporal and spectral domains is achievable in a smaller portion of the network area, corresponding to a smaller spatial MD reliability.
- Given  $p^h$  (i.e.,  $p_1$ ), there exists a limited variation between the minimum and maximum target MD reliability of the system. For example, considering  $p^h = 1 - 5 \times 10^{-8}$  in Fig. 4, the MD reliability can only change between 0.94 to 0.98 for all values of the spectral target reliability  $p^f$ . Besides, for any given  $p^h$ , there exists a maximum target reliability value  $\bar{p}^f$ , where selecting any  $p^f$  higher than this threshold does not deteriorate the overall reliability  $R^{\text{MD}}$  anymore. For example, as seen in Fig. 4, considering  $p^h = 1 - 2 \times 10^{-7}$  and  $m = 0$ , we have  $\bar{p}^f = 1 - 1 \times 10^{-3}$ .
- The higher-order MD reliability analysis can give insights into the impact level of the target reliability of each dimension on the overall MD reliability measure. For example, as seen in Fig. 4, going toward higher values of the spectral pdf shape factor (e.g.,  $m = 60$ ) increases the MD reliability at the cost of not effectively spreading the signal over the whole spectrum, leading to lower resiliency and higher risk of jamming.
- Fig. 5 shows another feature of the MD reliability of wideband THz communications. For any given spectral target reliability  $p^f$  in Scenario 2 wherein  $k(f)$  is not a monotonically increasing function in the available frequency range  $(\underline{f}^{(1)}, \bar{f})$ , the overall MD reliability is potentially optimal at some certain bandwidth value shown as filled circles, below and after which the MD reliability measure is smaller. The reason behind this relates to the mathematical formulation of  $P_2$  presented in (29) in Appendix I-B2. It is seen that given  $\mathcal{R}$ , for low values of the bandwidth,  $\mathcal{F}\mathcal{R}\sqrt{\exp(k(\mathcal{F})\mathcal{R})}$  in (29) is potentially decreasing in terms of  $\mathcal{F}$ . This is because the non-linearly decreasing term  $\sqrt{\exp(k(\mathcal{F})\mathcal{R})}$  for frequency range close to  $\underline{f}^{(1)}$  is potentially the dominant term

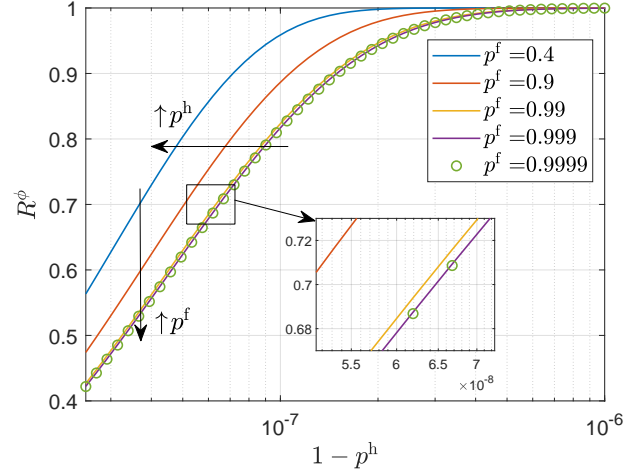


Fig. 3: Spatial MD reliability  $R^\phi$  versus temporal ( $p^h$ ) and spectral ( $p^f$ ) target reliabilities for  $m = 0$ .

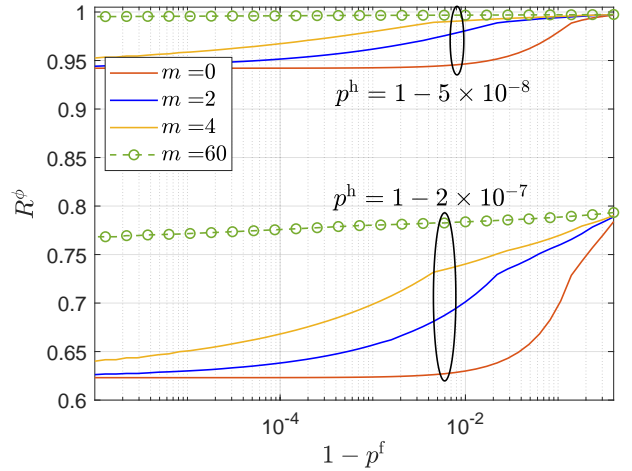


Fig. 4: Spatial MD reliability  $R^\phi$  versus temporal ( $p^h$ ) and spectral ( $p^f$ ) target reliabilities for different values of  $m$ .

compared to the linearly increasing term  $\mathcal{F}\mathcal{R}$ , leading to this function be finally decreasing in terms of  $\mathcal{F}$  for low bandwidth values. This increases the probability of  $P_2$  in (29), leading to a higher MD reliability. However, as the bandwidth increases, the function  $\mathcal{F}\mathcal{R}\sqrt{\exp(k(\mathcal{F})\mathcal{R})}$  becomes an increasing function of  $\mathcal{F}$  after some point  $\mathcal{F}^* \leq \arg\min_{f \in (\underline{f}^{(1)}, \bar{f})} \{k(f)\}$  since finally both exponential and linear terms will be monotonically increasing for frequencies higher than  $\arg\min_{f \in (\underline{f}^{(1)}, \bar{f})} \{k(f)\}$ , leading to lower success probability in (29) at such frequencies compared to that in  $\mathcal{F}^*$ , as shown in the Fig. 5.

## V. CONCLUSIONS

In this paper, we extended the meta distribution (MD) reliability analysis beyond conventional first-order spatiotemporal schemes. By structuring MD reliability in a hierarchical framework, we introduced the mathematical representation

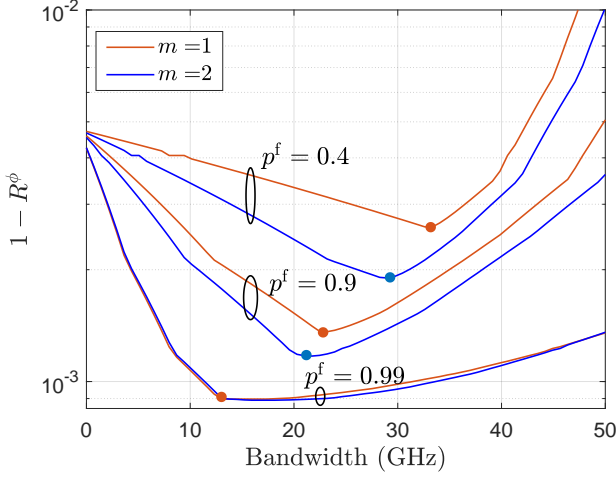


Fig. 5: Spatial MD reliability  $R^\phi$  versus bandwidth for different values of  $m$  and spectral target reliability  $p^f$ .

for higher-order MD reliability characterization, where the overall MD reliability is formulated in terms of target reliability thresholds in multiple domains. We also investigated various practical scenarios in wireless networks that benefit from this approach. Specifically, we conducted a second-order spatial-spectral-temporal MD reliability analysis for an ultra-wideband frequency-hopping spread spectrum THz network. Our analysis revealed how target reliabilities in the temporal and spectral domains influence the overall spatial MD reliability, providing nuanced insights into system performance that go beyond the capabilities of non-MD or first-order MD reliability analyses. For example, given desired success probability thresholds in the temporal and spectral domains, we showed that the spatial MD reliability is not a monotonically increasing function of the available bandwidth in THz frequencies. Instead, there exists an optimal bandwidth, beyond which the spatial MD reliability deteriorates. This underscores the importance of balancing bandwidth allocation to achieve optimal spatial reliability while meeting target temporal and spectral reliability requirements in THz wideband applications.

## APPENDIX I.

### ANALYTICAL SOLUTION TO THE CASE STUDY

In what follows, we present an analytical solution for calculating the MD reliability of the problem stated in Section IV. Considering the presented problem statement, from (4), we can formulate the MDs as follows:

$$P_1 = \mathbb{P}(t_l < t_{\text{th}} \mid \mathcal{R}, \mathcal{F}) \quad (11a)$$

$$P_2 = \mathbb{P}(P_1 > p_1 \mid \mathcal{R}) \quad (11b)$$

$$P_3 = \mathbb{P}(P_2 > p_2) \quad (11c)$$

In the first subsection, we present the solution for the case where the available spectrum is within a monotonically increasing portion of  $k(f)$ . Considering that many practical THz applications exploit the lower path loss associated with frequency bands near molecular absorption minima, in the

second subsection we elaborate on the solution for the more general case where  $k(f)$  is non-monotonic. Box 2 of Fig. 2 illustrates the frequency range corresponding to these two scenarios, wherein  $f \in [\underline{f}^{(2)}, \bar{f}]$  and  $f \in [\underline{f}^{(1)}, \bar{f}]$  correspond to the first and second scenarios respectively.

#### A. Scenario 1: Solution Scheme if $k(f)$ is Monotonically Increasing

In this case, we consider that the available bandwidth corresponds to a frequency range  $(\underline{f}, \bar{f})$  wherein  $k(f)$  is monotonically increasing.

1) *Calculation of  $P_1$* : From (8) and (11a) we can write  $P_1$  as follows:

$$\begin{aligned} P_1 &= \mathbb{P} \left( \log \left( 1 + \frac{c_0 \mathcal{H} e^{-k(\mathcal{F})\mathcal{R}}}{\mathcal{R}^2 \mathcal{F}^2} \right) > \frac{l}{W t_{\text{th}}} \mid \mathcal{R}, \mathcal{F} \right) \\ &= \mathbb{P} \left( \mathcal{H} > c_1 \mathcal{R}^2 \mathcal{F}^2 e^{-k(\mathcal{F})\mathcal{R}} \mid \mathcal{R}, \mathcal{F} \right), \end{aligned} \quad (12)$$

where

$$c_0 = \frac{P_T G_T G_R c^2}{(4\pi)^2 N_0 W}, \quad c_1 = c_0^{-1} \left( 2^{\frac{l}{W t_{\text{th}}}} - 1 \right). \quad (13)$$

The pdf of the small-scale fading is that of the Rician distribution with shape factor  $K$  as follows:

$$f_{\mathcal{H}}(x; K) = (K + 1) e^{-K - (K+1)x} I_0(\sqrt{4K(K+1)x}) \quad (14)$$

From (12) and (14),  $P_1$  can be obtained by calculating the cdf of  $\mathcal{H}$ . Following [20], this can be represented as follows:

$$\begin{aligned} P_1 &= \int_{c_1 \mathcal{R}^2 \mathcal{F}^2 e^{-k(\mathcal{F})\mathcal{R}}}^{\infty} f_{\mathcal{H}}(x; K) dx \\ &= Q_1 \left( \underbrace{\sqrt{2K}}_a, \underbrace{\mathcal{F} \mathcal{R} \sqrt{2c_1(K+1) \exp(k(\mathcal{F})\mathcal{R})}}_b \right), \end{aligned} \quad (15)$$

where  $Q_1$  is the first-order Marcum Q-function.

2) *Calculation of  $P_2$* : Noting that the Marcum Q-function is represented in the form of the integral of the modified Bessel function, following more analytical results in calculating  $P_2$  and  $P_3$  according to (11b) and (11c) involves the computation of multiple integrations of the modified Bessel function which is intractable using the original representation of the Marcum Q-function. To handle this, we use the exponential approximation of  $Q_1(a, b)$  represented as follows [21]:

$$\begin{aligned} \tilde{Q}_1(a, b) &= \exp \left( -e^{\sum_{n=0}^M (\mu_n \ln b + \nu_n) a^n} \right) \\ &= \exp \left( -e^{\nu(a)} b^{\mu(a)} \right), \end{aligned} \quad (16)$$

where  $\mu(a) = \sum_{n=0}^M \mu_n a^n$  and  $\nu(a) = \sum_{n=0}^M \nu_n a^n$ . Noting that  $a = \sqrt{2K}$  is a fixed argument in the represented Marcum Q-function, we can choose coefficients  $\boldsymbol{\mu} = [\mu_0, \dots, \mu_M]$  and  $\boldsymbol{\nu} = [\nu_0, \dots, \nu_M]$  in a way that the least square (LS) error function  $\mathcal{E}(a) = \int_0^\infty (Q_1(a, b) - \tilde{Q}_1(a, b))^2 db$  is minimized. For instance, considering  $a \in [1, 5]$  (corresponding to  $K \in [0.5, 12]$ ), the following coefficients have shown to result in a very tight approximation [21]:  $\boldsymbol{\mu} = [2.174, -0.592, 0.593, -0.092, 0.005]$  and  $\boldsymbol{\nu} = [-0.840, 0.327, -0.740, 0.083, -0.004]$ . For  $K = 2$ , corresponding to  $a = \sqrt{6}$  as considered in the numerical results,

this leads to  $\mu(a) = 3.1098$  and  $\nu(a) = -3.4032$ . Although choosing the given values minimizes the error  $\mathcal{E}(a)$  over the whole range of  $b \in [0, \infty)$ , such values might not be optimal in practice for calculating the MD reliability. This is attributed to the fact that we require a highly accurate approximation of the Marcum Q-function at certain points rather than the whole possible range of parameter  $b$ . To highlight this, note that we have  $P_2 = \mathbb{P}(P_1 > p_1 \mid \mathcal{R}) = \mathbb{E}\mathbf{1}(Q_1(a, b) > p_1 \mid \mathcal{R})$ . Therefore, it is highly important to have a highly accurate approximation at the argument value of  $b = b^*$  where  $Q_1(a, b^*) = p_1$  as this is the border argument value at which the value of  $\mathbf{1}(\cdot)$  switches between 0 and 1. Noting that the desired temporal target reliability  $p_1 \equiv p^h$  is generally a value very close to unity, we have obtained the optimal values as  $\mu(a) = 2.4246$  and  $\nu(a) = -3.3042$  for the values of  $p_1$  employed in our numerical results. Leveraging the approximate representation of  $Q_1$ , from (11b), (15) and (16), we can write  $P_2$  as

$$\begin{aligned} P_2 &= \mathbb{P}(P_1 > p_1 \mid \mathcal{R}) \\ &\approx \mathbb{P}\left(\exp\left(-e^{\nu(a)}\left(c_2 \mathcal{F}\mathcal{R}\sqrt{\exp(k(\mathcal{F})\mathcal{R})}\right)^{\mu(a)}\right) > p_1 \mid \mathcal{R}\right) \\ &= \mathbb{P}\left(\mathcal{F}\mathcal{R}\sqrt{\exp(k(\mathcal{F})\mathcal{R})} < \tilde{p}_1 \mid \mathcal{R}\right), \end{aligned} \quad (17)$$

where

$$c_2 = \sqrt{2c_1(K+1)}, \quad \tilde{p}_1 = \frac{1}{c_2} \times \left[-\frac{\ln(p_1)}{e^{\nu(a)}}\right]^{1/\mu(a)}. \quad (18)$$

Considering (17), given  $\mathcal{R}$ , let define  $\tilde{\mathcal{F}}(\mathcal{R})$  as follows:

$$\tilde{\mathcal{F}}(\mathcal{R}) = \left\{ \mathcal{F} \in (\underline{f}, \bar{f}) : \mathcal{F}\mathcal{R}\sqrt{\exp(k(\mathcal{F})\mathcal{R})} = \tilde{p}_1 \right\} \quad (19)$$

Noting the monotonically increasing assumption of  $k(f)$  for  $f \in (\underline{f}, \bar{f})$ , it can be easily verified that there exists a maximum number of one solution corresponding to  $\tilde{\mathcal{F}}(\mathcal{R})$  in the desired spectrum region. We will show later that there exists exactly one solution corresponding to each desired given value of  $\mathcal{R}$ .

Due to the non-linear representation of (17) as well as the non-linearity of the molecular absorption coefficient  $k(\cdot)$ , it is not generally possible to write a closed-form representation of  $\tilde{\mathcal{F}}$  in terms of  $\mathcal{R}$ . However, we will show that we may solve the problem without requiring the closed-form representation of  $\tilde{\mathcal{F}}(\mathcal{R})$ . Noting that we are studying a portion of the spectrum where  $k(f)$  is a monotonically increasing function, it can be verified from (19) that for a given  $\mathcal{R}$  we have

$$f\mathcal{R}\sqrt{\exp(k(f)\mathcal{R})} < \tilde{p}_1, \forall f \in (\underline{f}, \tilde{\mathcal{F}}(\mathcal{R})). \quad (20)$$

Considering this, together with the pdf expression of  $\mathcal{F}$  in (9),  $P_2(\mathcal{R})$  can be written as the cumulative distribution function (cdf) of  $\mathcal{F}$  with input argument  $\tilde{\mathcal{F}}(\mathcal{R})$ , which can be formulated as follows:

$$P_2(\mathcal{R}) = F_{\mathcal{F}}(\tilde{\mathcal{F}}(\mathcal{R})) = b_0 + \sum_{n=1}^{2m+1} \frac{b_n}{n} \left(\tilde{\mathcal{F}}(\mathcal{R})\right)^n, \quad \forall m \geq 0, \quad (21)$$

where  $b_n$  is the coefficient of  $x^n$  in the binomial expansion of (9), and  $b_0 = 1 - \sum_{n=1}^{2m+1} \frac{b_n}{n} (\bar{f})^n$  is obtained by noting

$F_{\mathcal{F}}(\bar{f}) = 1$ . For the simple case of  $m = 0$ , corresponding to the uniform distribution of  $\mathcal{F}$ , (21) simplifies as follows:

$$P_2(\mathcal{R}) = \left[\tilde{\mathcal{F}}(\mathcal{R}) - \underline{f}\right] / (\bar{f} - \underline{f}), \text{ if } m = 0 \quad (22)$$

We note that the expression of  $P_2(\mathcal{R})$  in (21) and even in the simple case of (22) is still not completely characterized, as the closed form solution of  $\tilde{\mathcal{F}}(\mathcal{R})$  is still not available.

3) *Calculation of  $P_3$* : First, consider the uniform distribution of  $\mathcal{F}$  (i.e.,  $m = 0$ ). In this case, From (11c) and (22) we have

$$P_3 = \mathbb{P}\left(\frac{\tilde{\mathcal{F}}(\mathcal{R}) - \underline{f}}{\bar{f} - \underline{f}} > p_2\right) = \mathbb{P}\left(\tilde{\mathcal{F}}(\mathcal{R}) > f_0\right), \quad (23)$$

where  $f_0 = p_2(\bar{f} - \underline{f}) + \underline{f}$ . From (19) it is seen that  $\tilde{\mathcal{F}}(\mathcal{R})$  is a monotonically decreasing function of  $\mathcal{R}$ . Therefore (23) results in

$$P_3 = \mathbb{P}(\mathcal{R} < \tilde{\mathcal{F}}^{-1}(f_0)). \quad (24)$$

One can verify that (24) also holds for all  $m \geq 0$ , however for this more general case,  $f_0$  can be found as the solution of the following equation:

$$b_0 + \sum_{n=1}^{2m+1} \frac{b_n}{n} (f_0)^n = p_2, \quad \forall m \geq 0. \quad (25)$$

Noting that the left side of the equality corresponds to a cdf which is a monotonically increasing function, there is a unique solution to  $f_0 \in [\underline{f}, \bar{f}]$  which can easily be obtained using numerical methods. Once  $f_0$  is calculated, we can compute  $R_0 = \tilde{\mathcal{F}}^{-1}(f_0)$  from (19) by putting  $\tilde{\mathcal{F}} = f_0$  and finding  $R_0$  as the closed form solution of

$$R_0^2 \exp(k(f_0)R_0) = (\tilde{p}_1/f_0)^2. \quad (26)$$

Noting that the solution to the equation  $xe^{cx} = b$  can be represented as  $x = \frac{1}{c}W_0(bc)$ , where  $W_0$  is the principal branch of Lambert  $W$  function, after some mathematical manipulations, we obtain  $R_0$  as follows:

$$R_0 = \frac{2}{k(f_0)}W_0\left(\frac{k(f_0)\tilde{p}_1}{2f_0}\right) \quad (27)$$

Finally, the MD reliability is obtained as follows:

$$\begin{aligned} R^{\text{MD}} \equiv P_3 &= \int_0^{R_0} f_{\mathcal{R}}(x)dx \\ &= 1 - \exp\left(\frac{-4\lambda\pi}{k^2(f_0)} \times W_0^2\left(\frac{k(f_0)\tilde{p}_1}{2f_0}\right)\right) \end{aligned} \quad (28)$$

### B. Scenario 2: Solution Scheme if $k(f)$ is not Monotonic

Given that many practical THz applications exploit lower path loss associated with frequency bands near molecular absorption minima, here we consider a scenario where the channel gain  $k(f)$  is non-monotonic within the frequency range  $(\underline{f}, \bar{f})$ . Specifically, we consider the case  $\underline{f} = \underline{f}^{(1)}$  illustrated in Fig. 2, where  $k(f)$  contains a local minimum in the spanning frequency range.

1) *Calculation of  $P_1$* : This is achieved using (15) as described in Appendix I-A1.



2) *Calculation of  $P_2$* : Similar to the steps taken in Appendix I-A2,  $P_2$  is obtained from the following equation:

$$P_2 = \mathbb{P} \left( \underbrace{\mathcal{FR} \sqrt{\exp(k(\mathcal{F})\mathcal{R})}}_{\mathcal{A}(\mathcal{F};\mathcal{R})} < \tilde{p}_1 \mid \mathcal{R} \right), \quad (29)$$

where  $\tilde{p}_1$  is given in (18). To solve (29), first we investigate the solutions of (19) denoted by  $\mathcal{F}_m(\mathcal{R})$  where  $m$  indexes the solutions in ascending order of magnitude. Considering the behavior of  $k(f)$  for  $f \in [\underline{f}, \bar{f}]$  where  $k(\cdot)$  can initially follow a monotonically decreasing and then a monotonically increasing behavior, one can verify that we may have (a) zero, (b) one, or (c) two solution values. In what follows we investigate each case:

- *Case (a)*: If there exists no solution to (19), the event  $\mathcal{A}(f; \mathcal{R})$  in (29) holds the same true/false value for all  $f \in (\underline{f}, \bar{f})$ . Therefore, we may represent the frequency range where the corresponding event holds true as  $(\tilde{\mathcal{F}}_1(\mathcal{R}), \tilde{\mathcal{F}}_2(\mathcal{R}))$ , where

$$\begin{aligned} \tilde{\mathcal{F}}_1(\mathcal{R}) &= \underline{f} \\ \tilde{\mathcal{F}}_2(\mathcal{R}) &= \underline{f} + (\bar{f} - \underline{f}) \times \mathbf{1}(\underline{f}\mathcal{R} \sqrt{\exp(k(\underline{f})\mathcal{R})} < \tilde{p}_1 \mid \mathcal{R}). \end{aligned} \quad (30)$$

- *Case (b)*: If there exists one solution to (19), namely  $\mathcal{F}_1$ , the event  $\mathcal{A}(f; \mathcal{R})$  in (29) holds same value for  $f \in [\underline{f}, \mathcal{F}_1]$  and the complemented value for  $f \in [\mathcal{F}_1, \bar{f}]$ . Therefore, we may represent the frequency range where the corresponding event holds true as  $(\tilde{\mathcal{F}}_1(\mathcal{R}), \tilde{\mathcal{F}}_2(\mathcal{R}))$ , where

$$\begin{aligned} \tilde{\mathcal{F}}_1(\mathcal{R}) &= \mathcal{F}_1 + (\underline{f} - \mathcal{F}_1) \times \mathbf{1}(\underline{f}\mathcal{R} \sqrt{\exp(k(\underline{f})\mathcal{R})} < \tilde{p}_1 \mid \mathcal{R}) \\ \tilde{\mathcal{F}}_2(\mathcal{R}) &= \bar{f} + (\mathcal{F}_1 - \bar{f}) \times \mathbf{1}(\underline{f}\mathcal{R} \sqrt{\exp(k(\underline{f})\mathcal{R})} < \tilde{p}_1 \mid \mathcal{R}). \end{aligned} \quad (31)$$

- *Case (c)*: Finally, for the case where there exist two solutions to (19), namely  $\mathcal{F}_1$  and  $\mathcal{F}_2$  where  $\mathcal{F}_1 \leq \mathcal{F}_2$ , the event  $\mathcal{A}(f; \mathcal{R})$  in (29) holds false for any frequency  $f > \mathcal{F}_2$  due to the behavior of  $k(\cdot)$  corresponding to Scenario 2. Therefore, the frequency range where the corresponding event holds true is  $(\tilde{\mathcal{F}}_1(\mathcal{R}), \tilde{\mathcal{F}}_2(\mathcal{R}))$ , where

$$\tilde{\mathcal{F}}_1(\mathcal{R}) = \mathcal{F}_1, \quad \tilde{\mathcal{F}}_2(\mathcal{R}) = \mathcal{F}_2. \quad (32)$$

After obtaining the minimum and maximum thresholds  $\tilde{\mathcal{F}}_1(\mathcal{R})$  and  $\tilde{\mathcal{F}}_2(\mathcal{R})$ ,  $P_2(\mathcal{R})$  is formulated from (21) as

$$\begin{aligned} P_2(\mathcal{R}) &= F_{\mathcal{F}}(\tilde{\mathcal{F}}_2(\mathcal{R})) - F_{\mathcal{F}}(\tilde{\mathcal{F}}_1(\mathcal{R})) = \\ &= \sum_{n=1}^{2m+1} \frac{b_n}{n} \left[ \left( \tilde{\mathcal{F}}_2(\mathcal{R}) \right)^n - \left( \tilde{\mathcal{F}}_1(\mathcal{R}) \right)^n \right], \forall m \geq 0. \end{aligned} \quad (33)$$

For the simple case of uniform distribution ( $m = 0$ ), this reduces to  $P_2(\mathcal{R}) = [\tilde{\mathcal{F}}_2(\mathcal{R}) - \tilde{\mathcal{F}}_1(\mathcal{R})]/(\bar{f} - \underline{f})$ .

---

**Algorithm 1** : Calculation of the spatial-spectral-temporal MD reliability for Scenario 2

---

**Output:**

$$R^{\text{MD}};$$

**Initialization:**

- 1: Compute  $c_0, c_1, c_2, \tilde{p}_1$  from (13) and (18);
- 2: Let  $R^{\text{MD}} = 0, r = 0$  and  $\Delta r$  be a small value;

**Main Procedure:**

- 3: **do**
  - 4:    $r = r + \Delta r$ ;
  - 5:   Calculate the set of solutions of (19) where  $M \in \{0, 1, 2\}$  is the total number of solution values obtained;
  - 6:   Let  $\tilde{\mathcal{F}}_1(r)$  and  $\tilde{\mathcal{F}}_2(r)$  be obtained from (30), (31), or (32), if  $M = 0, M = 1$ , or  $M = 2$  respectively.
  - 7:   **if**  $\left( \sum_{n=1}^{2m+1} \frac{b_{n-1}}{n} \left[ \left( \tilde{\mathcal{F}}_2(r) \right)^n - \left( \tilde{\mathcal{F}}_1(r) \right)^n \right] > p_2 \right)$
  - 8:      $R^{\text{MD}} = R^{\text{MD}} + 2\pi\lambda r \exp(-\lambda\pi r^2)\Delta r$ ;
  - 9:   **end if**
  - 10: **loop until** convergence
- 

*C. Calculation of  $P_3$* :

Once  $\tilde{\mathcal{F}}_1$  and  $\tilde{\mathcal{F}}_2$  are calculated considering any of the corresponding cases of (a), (b) and (c) elaborated in the previous part, the MD reliability can be calculated as follows:

$$\begin{aligned} P_3 &= \mathbb{P}(P_2 > p_2) = \mathbb{E} \mathbf{1}(P_2 > p_2) \\ &= \int_0^\infty \mathbf{1}(P_2(r) > p_2) f_{\mathcal{R}}(r) dr \\ &= \int_0^\infty \mathbf{1} \left( \sum_{n=1}^{2m+1} \frac{b_{n-1}}{n} \left[ \left( \tilde{\mathcal{F}}_2(r) \right)^n - \left( \tilde{\mathcal{F}}_1(r) \right)^n \right] > p_2 \right) \times \\ &\quad 2\pi\lambda r \exp(-\lambda\pi r^2) dr. \end{aligned} \quad (34)$$

Noting that (34) can not be solved in a closed-form scheme, we present the numerical procedure for obtaining the MD reliability in Algorithm 1.

## REFERENCES

- [1] M. Haenggi, "Meta Distributions—Part 1: Definition and Examples," *IEEE Communications Letters*, vol. 25, no. 7, pp. 2089–2093, 2021.
- [2] M. Haenggi, "Meta Distributions—Part 2: Properties and Interpretations," *IEEE Comm. Lett.*, vol. 25, no. 7, pp. 2094–2098, 2021.
- [3] S. Kalamkar and M. Haenggi, "Per-Link Reliability and Rate Control: Two Facets of the SIR Meta Distribution," *IEEE Wireless Communications Letters*, vol. 8, no. 4, pp. 1244–1247, 2019.
- [4] S. S. Kalamkar and M. Haenggi, "Simple Approximations of the SIR Meta Distribution in General Cellular Networks," *IEEE Transactions on Communications*, vol. 67, no. 6, pp. 4393–4406, 2019.
- [5] M. Haenggi, "The Meta Distribution of the SIR in Poisson Bipolar and Cellular Networks," *IEEE Transactions on Wireless Communications*, vol. 15, no. 4, pp. 2577–2589, 2016.
- [6] M. Salehi, A. Mohammadi, and M. Haenggi, "Analysis of D2D Underlaid Cellular Networks: SIR Meta Distribution and Mean Local Delay," *IEEE Transactions on Communications*, vol. 65, no. 7, pp. 2904–2916, 2017.
- [7] Q. Cui, X. Yu, Y. Wang, and M. Haenggi, "The SIR Meta Distribution in Poisson Cellular Networks With Base Station Cooperation," *IEEE Transactions on Communications*, vol. 66, no. 3, pp. 1234–1249, 2018.
- [8] M. Salehi, H. Tabassum, and E. Hossain, "Meta Distribution of SIR in Large-Scale Uplink and Downlink NOMA Networks," *IEEE Transactions on Communications*, vol. 67, no. 4, pp. 3009–3025, 2019.
- [9] J. Tang, G. Chen, and J. P. Coon, "Meta distribution of the secrecy rate in the presence of randomly located eavesdroppers," *IEEE Wireless Communications Letters*, vol. 7, no. 4, pp. 630–633, 2018.

- [10] Z. Wang and J. Zheng, "Rate Meta Distribution of Downlink Base Station Cooperation for Cellular-Connected UAV Networks," *IEEE Communications Letters*, vol. 27, no. 2, pp. 756–760, 2023.
- [11] Y. Quan, M. Coupechoux, and J.-M. Kélif, "Rate Meta-Distribution in Millimeter Wave URLLC Device-to-Device Networks with Beam Misalignment," *IEEE Transactions on Vehicular Technology*, vol. 74, no. 1, pp. 657–673, 2024.
- [12] N. Deng and M. Haenggi, "The Energy and Rate Meta Distributions in Wirelessly Powered D2D Networks," *IEEE Journal on Selected Areas in Communications*, vol. 37, no. 2, pp. 269–282, 2019.
- [13] A. Gomes, J. Kibilda, and L. A. DaSilva, "Assessing the Spectrum Needs for Network-Wide Ultra-Reliable Communication With Meta Distributions," *IEEE Comm. Lett.*, vol. 27, no. 8, pp. 2242–2246, 2023.
- [14] S. Zhou, H. Dai, H. Sun, G. Tan, and B. Ye, "On the Deployment of Clustered Power Beacons in Random Wireless Powered Communication," *IEEE Trans. Veh. Technol.*, vol. 72, no. 2, pp. 2424–2438, 2023.
- [15] 3GPP, "5G; Study on scenarios and requirements for next generation access technologies (3GPP TR 38.913 version 18.0.0 Release 18)," 3GPP, Technical Report (TR), 2024.
- [16] H. Tabassum, M. Salehi, and E. Hossain, "Fundamentals of Mobility-Aware Performance Characterization of Cellular Networks: A Tutorial," *IEEE Commu. Surveys & Tutorials*, vol. 21, no. 3, pp. 2288–2308, 2019.
- [17] J. Kokkonen, J. Lehtomäki, and M. Juntti, "Simplified molecular absorption loss model for 275–400 gigahertz frequency band," in *12th European Conference on Antennas and Propagation (EuCAP 2018)*, 2018, pp. 1–5.
- [18] M. A. Saeidi, H. Tabassum, and M. Alizadeh, "Molecular Absorption-Aware User Assignment, Spectrum, and Power Allocation in Dense THz Networks with Multi-Connectivity," *IEEE Transactions on Wireless Communications*, vol. 23, no. 11, p. 16404–16420, 2024.
- [19] C. Wang and Y. J. Chun, "Stochastic Geometric Analysis of the Terahertz (THz)-mmWave Hybrid Network With Spatial Dependence," *IEEE Access*, vol. 11, pp. 25063–25076, 2023.
- [20] M. K. Simon and M.-S. Alouini, *Digital Communication over Fading Channels*. John Wiley & Sons, 2005.
- [21] M. Z. Bocus, C. P. Dettmann, and J. P. Coon, "An Approximation of the First Order Marcum Q-Function with Application to Network Connectivity Analysis," *IEEE Communications Letters*, vol. 17, no. 3, pp. 499–502, 2013.